Evolution of a Surface-Roughness Spectrum Caused by Stress in Nanometer-Scale Chemical Etching

K.-S. Kim, J. A. Hurtado, and H. Tan
Division of Engineering, Brown University, Providence, Rhode Island 02912
(Received 10 June 1999)

It is reported that a flat free surface of a stressed solid is configurationally unstable under chemical etching and the surface roughness grows with different rates for different spatial frequencies. The theory described in this Letter predicts that with a shallow chemical etching the roughness with spatial frequency below a critical value grows while the roughness of higher frequency decays. The theory was verified via an atomic force microscope experiment with aluminum. This study provides a simple experimental method to measure stress in metals and ceramics.

PACS numbers: 68.35.Ct, 46.80.+j, 68.45.–v, 81.65.Cf

The phenomenon of stress-induced roughening of solid surfaces has recently gained great attention [1], especially because of its relevance in the morphological instability of flat surfaces and island formation during heteroepitaxial growth of thin films. There are two distinctive atomic-level mechanisms which allow variation of the surface configuration. One is the case of direct addition and removal of atoms on the surface from and to the surroundings of the surface. Chemical etching belongs to this case. The other is the case in which atoms move along the surface itself. In the latter case a gradient in the chemical potential results in diffusive mass transport along the surface [1]. This phenomenon is particularly relevant for processes characterized by high stress, high temperature, and small-size scales, such as during growth of heteroepitaxial thin films. The general observation is that a flat surface under stress is unstable against diffusional perturbations with a sufficiently large wavelength λ (or small wave number $\omega = 2\pi/\lambda$); there exists a critical wave number ω_{cr} below which diffusional perturbations grow and above which they decay. A similar behavior is expected in chemical etching processes. The stress-induced surface roughening in a shallow chemical etching is analyzed, in this Letter, for isotropic homogeneous solids. The analysis shows that the stress roughening in this case also has the same critical wave number ω_{cr}; however, the frequency-spectrum dependence of the growth (or decay) rate of the roughness is different for the two cases. This analysis provides a simple stress dependent function of the growth rate of the surface roughness for general two-dimensional frequency spectrum. An atomic force microscope (AFM) has been used for direct measurements of the surface topography of a stressed aluminum sample between two etching steps. The surface topographies are then processed to reveal the frequency dependence of stress-induced roughening in chemical etching. This Letter provides, for the first time, direct experimental verification of this frequency dependence.

(a) Etching kinetics and surface evolution.—The geometry of chemical etching is depicted in Fig. 1. An elastic solid subject to a uniform biaxial stress field $\boldsymbol{\sigma}$ is covered by an etching solution. The solid is considered to be isotropic and homogeneous, with shear modulus μ and Poisson's ratio ν, and always in mechanical equilibrium. The tendency of the interface to change the shape of its reference configuration is represented by the chemical potential [2,3] along the surface $\chi(s) = \Omega[g_0 + \gamma\kappa(s) + w(s)]$, where s indicates a point on the surface, Ω is the atomic volume, g_0 is the electrochemical potential of the etching reaction, γ is the interface energy density of the solid-etchant interface, κ is the curvature (positive in sign for a concave surface), and w is the strain energy density along the solid surface. As the surface configuration is varied, the positive interface energy tends to flatten the surface while the positive strain energy is inclined to roughen the surface, changing the chemical potential in opposite directions. This competition depends on the spatial frequency of the roughness. The speed of etching is assumed to be directly proportional to $\chi(s)$, thus

$$\partial H/\partial t = M(g_0 + \gamma\kappa + w)\sqrt{1 + |\nabla H|^2}, \qquad (1)$$

where H is the height of the interface as shown in Fig. 1, M is the linear kinetic constant of etching, and ∇ denotes the two-dimensional gradient operator. The projected average

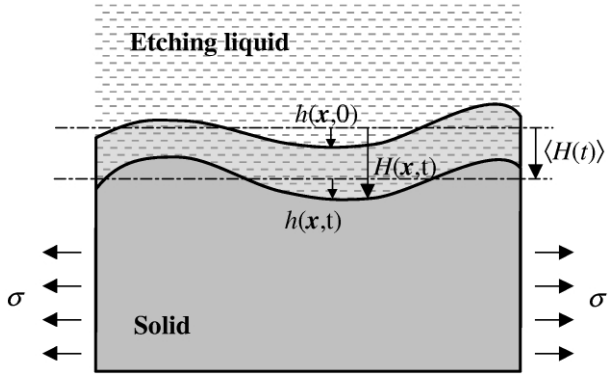

FIG. 1. Schematic of chemical etching of a solid surface under stress $\boldsymbol{\sigma}$. The height and roughness of the surface, at time t and position $\boldsymbol{x}$, are represented as $H(\boldsymbol{x}, t)$ and $h(\boldsymbol{x}, t)$, respectively.

 0031-9007/99/83(19)/3872(4)$15.00

of the chemical potential is maintained constant [4] during surface evolution; i.e., $\langle g_0 + \gamma\kappa + w\rangle = g_0 + w_0$, where w_0 is the strain energy density of the uniform state for a perfectly flat interface. The operator $\langle\ldots\rangle$ denotes the projected average over the entire interface between the etching liquid and the solid. The function $h(\boldsymbol{x}, t) = H(\boldsymbol{x}, t) - \langle H(\boldsymbol{x}, t)\rangle$ represents the roughness. For a shallow chemical etching of a nearly flat surface, $|\nabla h| \ll 1$, the roughness can be treated as a perturbed state of the flat surface. The curvature of the surface can be approximated as $\kappa \approx \nabla^2 h$ where $\nabla^2 = \partial^2/\partial x_1^2 + \partial^2/\partial x_2^2$. Thus, the first-order evolution equation of the roughness for $|\nabla h| \ll 1$ is

$$\partial h/\partial t = M\{\gamma\nabla^2 h + \Delta w\}, \tag{2}$$

where $\Delta w = w - w_0$. When the surface is subjected to a uniform planar stress field $\boldsymbol{\sigma}$, the change in strain energy caused by the surface fluctuation is, to a first-order approximation,

$$\Delta w(\boldsymbol{x}) = -\int_{S(\boldsymbol{\xi})} \boldsymbol{\sigma}{:}\nabla\boldsymbol{K}(\boldsymbol{x} - \boldsymbol{\xi}) \cdot \boldsymbol{\sigma} \cdot \nabla h(\boldsymbol{\xi})\, d\xi_1\, d\xi_2\,. \tag{3}$$

Here $S(\boldsymbol{\xi})$ indicates the domain of the projected surface and $\boldsymbol{K}(\boldsymbol{x})$ is the surface Green function of the Cerruti solution [5] with components

$$K_{kl}(\boldsymbol{x}) = \frac{1}{2\pi\mu}\left(\frac{1-\nu}{r}\,\delta_{kl} + \frac{\nu x_k x_l}{r^3}\right) \qquad k, l = 1, 2\,, \tag{4}$$

where δ_{kl} is the two-dimensional Kronecker's delta, and $r = (x_1^2 + x_2^2)^{1/2}$. After Fourier transforming (2) with respect to $\boldsymbol{x}$ and integrating in time t, we find

$$\ln[\hat{h}(\boldsymbol{\omega}, t)/\hat{h}(\boldsymbol{\omega}, 0)] = -\bar{M}(t)\,[\gamma\omega^2 - A(\boldsymbol{\sigma}, \boldsymbol{n})\omega], \tag{5}$$

for $\omega\|h\| \ll 1$, where $\|h\|$ is a norm of h and $\bar{M}(t) = \int_0^t M(\tau)\, d\tau$ is proportional to the net amount of etching. The "hat" symbol on h indicates the magnitude of the Fourier transformation. The wave vector of the roughness spectrum is represented by $\boldsymbol{\omega} = \omega\boldsymbol{n}$, where ω is the absolute wave number and $\boldsymbol{n}$ is a unit directional vector on the surface. The time dependence of the kinetic constant $M(t)$, which varies during the etching process due to dilution of the etchant and temperature variation, does not influence the functional form of (5) with respect to ω within the accuracy of the first-order theory. $A(\boldsymbol{\sigma}, \boldsymbol{n})$ is a positive definite function that can be expressed in a simple form in terms of the normal and shear components, t_n and t_s, of the stress vector $\boldsymbol{t} = \boldsymbol{\sigma} \cdot \boldsymbol{n}$, as

$$A(\boldsymbol{\sigma}, \boldsymbol{n}) = [(1-\nu)t_n^2 + t_s^2]/\mu\,, \tag{6}$$

where $t_n = \boldsymbol{n}^T \cdot \boldsymbol{t}$ and $t_s = (|\boldsymbol{t}|^2 - t_n^2)^{1/2}$. The function $\Psi(\boldsymbol{\omega}; \boldsymbol{\sigma}) \equiv (1/\bar{M})\ln[\hat{h}(\boldsymbol{\omega}, t)/\hat{h}(\boldsymbol{\omega}, 0)]$ of roughness evolution, given by (5), is plotted in Fig. 2 for five typical stress states, A through E, which are indicated on the principal-stress (σ_1, σ_2) plane in the figure, top left. Note that $\Psi(\boldsymbol{\omega}; \boldsymbol{\sigma})$ has center symmetry with respect to the origin of the $\boldsymbol{\sigma}$ plane. For $\sigma_1 \neq \sigma_2$, $\Psi(\boldsymbol{\omega}; \boldsymbol{\sigma})$ has two or four peaks on the $\boldsymbol{\omega}$ plane, depending on whether the product $[\sigma_1 + (1-2\nu)\sigma_2][\sigma_2 + (1-2\nu)\sigma_1]$ is greater or less than zero, respectively. The region, on the $\boldsymbol{\sigma}$ plane, corresponding to four peaks is illustrated as shaded areas in the figure. For $\sigma_1 = \sigma_2$, $\Psi(\boldsymbol{\omega}; \boldsymbol{\sigma})$ has peaks as a circular ridge on the $\boldsymbol{\omega}$ plane, Fig. 2(A). In these plots, 2(A)–2(E), the (ω_1, ω_2) axes are aligned with the principal stress directions (σ_1, σ_2). Figure 2 shows that the directions of the valleys of $\Psi(\boldsymbol{\omega}; \boldsymbol{\sigma})$ always correspond to the principal directions of the stress. The locus of $\Psi(\boldsymbol{\omega}; \boldsymbol{\sigma}) = 0$, except for $\omega = 0$, is the trajectory of the critical wave number, $\omega_{cr} = A(\boldsymbol{\sigma}, \boldsymbol{n})/\gamma$, shown as a white contour in Figs. 2(A)–2(E). Any Fourier component of the roughness in the $\boldsymbol{n}$ direction with wave number ω greater (smaller) than ω_{cr} will decay (grow) as the surface is chemically etched. Along the principal directions

$$\omega_{cr} = (1-\nu)\sigma_p^2/\mu\gamma\,, \tag{7}$$

where σ_p is the principal stress and ω_{cr} is identified as the peak-to-peak distance along the principal direction on the $\boldsymbol{\omega}$ plane. According to (7), the interface energy γ can be obtained from a uniaxial-tension calibration experiment where σ_p is known and ω_{cr} is inferred from the roughness-evolution measurements during etching. Once γ is determined, the magnitudes of the principal stresses of an unknown stress state can be obtained by measuring the critical wave number. The absolute sign of the stress state can be resolved by an auxiliary test, knowing the sign of an additional loading to the stress state.

Experimental verification.—We carried out an experiment in order to test the theory. The material chosen for the experiment was a structural aluminum alloy, frequently used for computer hard disks. The etchant employed in this experiment was the Keller reagent, a common aluminum-alloy etchant: HF 48% (2 ml), HCl (3 ml), HNO_3 (5 ml), H_2O (190 ml). We measured the topography with a commercial AFM (PSI AutoProbe CP with Multitask probe head) in contact mode, with a Si_3N_4 tip. The instrument has the capability to return to a previously scanned area, which allows us to retract the tip from the specimen, etch the scanning area, and bring the tip back to the same location for a subsequent scan. An alternative method is to use a microcell for direct measurements in the etching liquid. This last technique has been successfully used for the study of the etching kinetics of SiO_2-Si structures [6] in HF solution.

The specimen used in this experiment is depicted in the left inset of Fig. 3. The notch in the specimen was opened by deforming the ligament plastically with the load P as shown in the figure. Then the load P was removed, leaving a high residual stress field in the vicinity of the notch end. The specimen with the residual stress was placed in the AFM, and the etching experiment was carried out in two regions near the notch, T and S, shown in the figure. A near-equibiaxial-tension field is

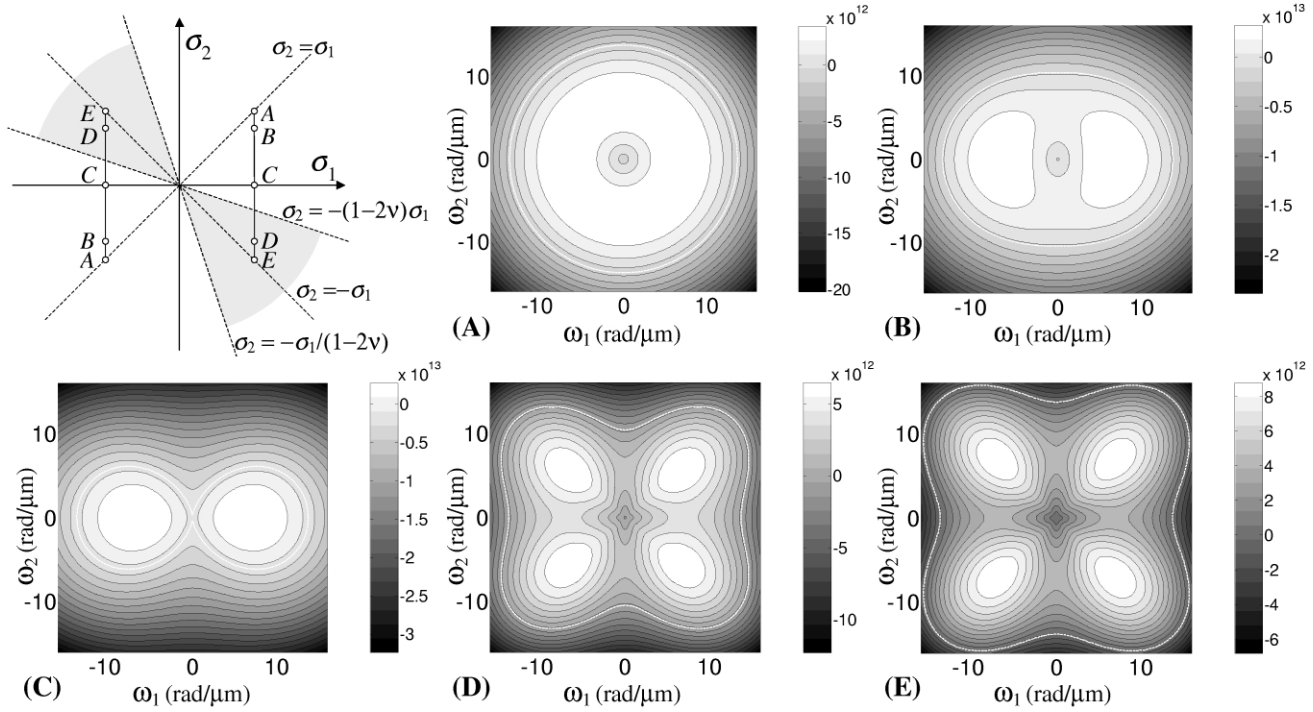

FIG. 2. Predictions for the roughness-evolution function $\Psi(\boldsymbol{\omega};\boldsymbol{\sigma})$ for five different stress states: (A) equibiaxial, $\sigma_1 = \sigma_2 = \pm 230$ MPa; (B) near equibiaxial, $\sigma_1 = \pm 230$ MPa, $\sigma_2 = \pm 200$ MPa; (C) uniaxial, $\sigma_1 = \pm 230$ MPa, $\sigma_2 = 0$ MPa; (D) near pure-shear, $\sigma_1 = \pm 230$ MPa, $\sigma_2 = \mp 200$ MPa; (E) pure-shear, $\sigma_1 = \pm 230$ MPa, $\sigma_2 = \mp 230$ MPa. The stress states, *A* through *E*, are illustrated on the principal-stress (σ_1, σ_2) plane, top left. For these plots $\gamma = 0.1$ J/m^2, $\nu = 0.3$, and $\mu = 27$ GPa have been used.

anticipated in region *T*, while a high shear-stress field is expected in region *S*. These regions were etched *in situ* in the AFM, then scanned. The first-step scans of the topography, shown in Figs. 3(T.1) and 3(S.1), were used as the reference states $h(\boldsymbol{x}, 0)$ for our calculations. The AFM tip was retreated in order to etch a second time, then brought back to the same locations. The second-step scans of the topography, $h(\boldsymbol{x}, t)$, are shown in Figs. 3(T.2) and 3(S.2). The topographic measurements were made with 256 by 256 digital sampling of an area of 25 μm by 25 μm at each region of *T* and *S*. The functions $\hat{h}(\boldsymbol{\omega}, t)$ and $\hat{h}(\boldsymbol{\omega}, 0)$ were evaluated numerically using a fast Fourier transformation (FFT) code. Finally the function $\ln[\hat{h}(\boldsymbol{\omega}, t)/\hat{h}(\boldsymbol{\omega}, 0)]$, which is equal to $\bar{M}\Psi(\boldsymbol{\omega};\boldsymbol{\sigma})$, is plotted in Figs. 4(T) and 4(S) after a numerical (finite-window-size average) smoothing of the data. The peaks

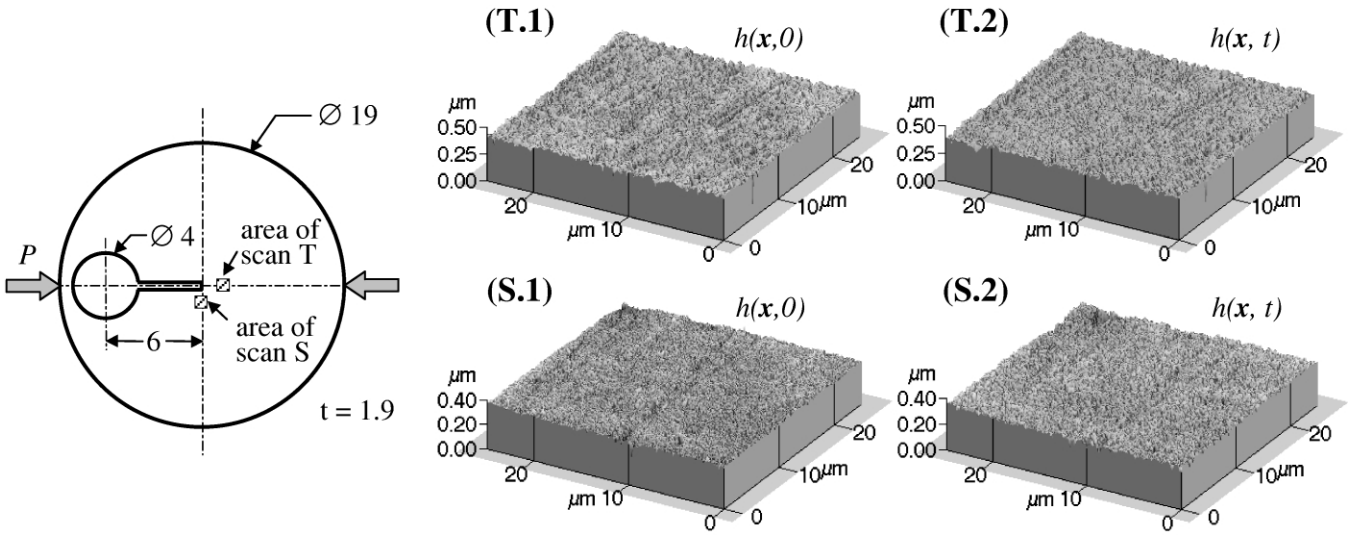

FIG. 3. Specimen geometry of high residual stress for AFM scanning (units in mm), left inset; the squares indicating the areas of scan at *T* and *S* are not in scale. AFM measurements of surface topography before [(T.1) and (S.1)] and after [(T.2) and (S.2)] etching for an aluminum specimen with residual stresses at *T* and *S*.

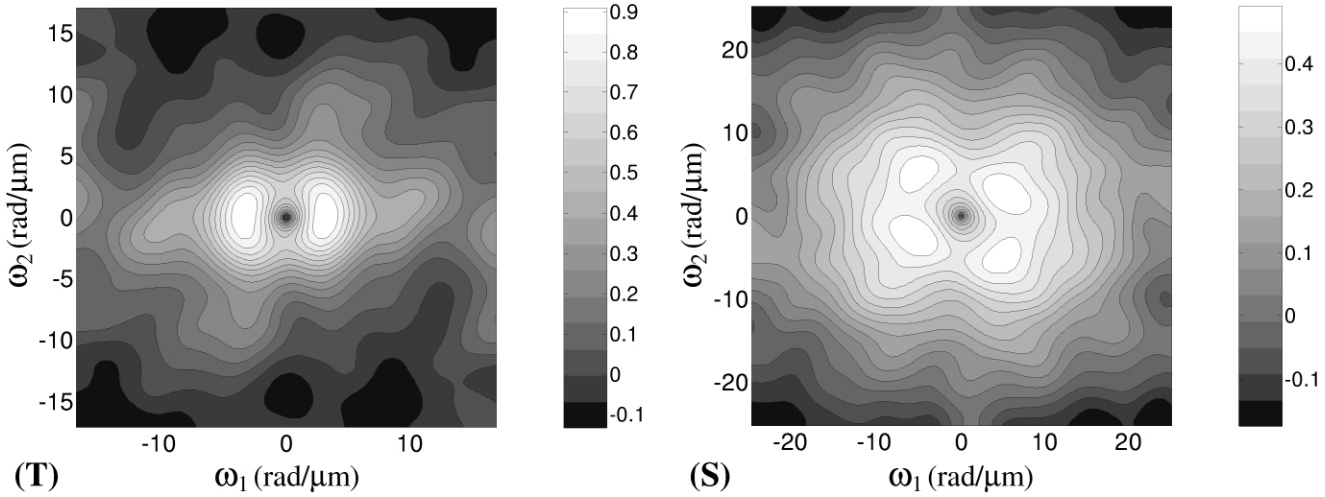

FIG. 4. Experimentally measured values of the function $\ln[\hat{h}(\boldsymbol{\omega}, t)/\hat{h}(\boldsymbol{\omega}, 0)]$ for the roughness data of an area of 25 μm by 25 μm for the scans at T and S. The two peaks for T and the four peaks for S clearly indicate the presence of near-equibiaxial stress at T and high shear stress at S in the solid.

of Figs. 4(T) and 4(S) appear close to the predictions in Figs. 2(B) and 2(D) for near-equibiaxial-tension stress and near-pure-shear stress, respectively. The results are remarkable, considering that the specimen is anisotropic and atomistically inhomogeneous within each test area; both for T and for S the scanning was made within a single grain for which the crystallographic orientations were not identified. The distances between the peaks in the frequency domain are in the order of $10\ \mathrm{rad}/\mu\mathrm{m}$ which corresponds to approximately 200 MPa for a reasonable choice of material parameters in (7): $\mu = 27$ GPa, $\nu = 0.3$, and the interface energy $\gamma = 0.1\ \mathrm{J/m^2}$. This stress estimation is within a reasonable range of an expected stress level near a plastically deformed notch in an aluminum-alloy specimen of 400 MPa yield strength.

A systematic series of tests were carried out with successive etching at a same location with different scan sizes of 25×25 and $10 \times 10\ \mu\mathrm{m}^2$. The stress measurement was remarkably reproducible irrespective of the scan-size variation and successive etching; however, the resolution on the frequency plane goes down for a smaller area of scan. With small scan sizes the behavior of the evolution function could be observed at a high frequency range where the shallow-etching condition (or low-frequency approximation), $\omega\|h\| \ll 1$, is no longer valid; this range is out of the scope of this paper. On the other hand, some effects of material anisotropy are still observable at the low-frequency range of shallow etching. For example, the contours in Fig. 4(S) develop 12 ears as the wave number increases, which indicates that the interface energy of our sample is anisotropic. Within the frequency range of shallow etching the behavior of the evolution function for large wave numbers is mainly governed by the interface-energy driven flattening of the surface, as indicated by the ω^2 term in (5), which would make the level contours circular for large ω, if it were isotropic. While the effects of anisotropy and inhomogeneity of the material need to be studied further, the results provide the first experimental evidence of the frequency dependence of stress-induced roughening under the condition of shallow chemical etching. The analysis and the experimental procedure reported in this Letter provide a new experimental technique to measure stress in metals and ceramics with high spatial resolution. It may be called the surface roughness-evolution spectroscopy.

This work was supported in part by the MRSEC Program of NSF under Award No. DMR-9632524, the IMRE in Singapore, and the Ford Motor Company.

[1] R. J. Asaro and W. A. Tiller, Metall. Trans. **3**, 1789 (1972); M. A. Grinfeld, Sov. Phys. Dokl. **31**, 831 (1986); J. Nonlinear Sci. **3**, 35 (1993); D. J. Srolovitz, Acta Metall. **37**, 621 (1989); W. D. Nix, Metall. Trans. **20A**, 2217 (1989); B. J. Spencer, P. W. Voorhees, and S. H. Davis, Phys. Rev. Lett. **67**, 3696 (1991); H. Gao, J. Mech. Phys. Solids **39**, 443 (1991); L. B. Freund, Int. J. Solids Struct. **32**, 911 (1995); J. Grilhe, Europhys. Lett. **23**, 141 (1993); C. W. Snyder, B. G. Orr, D. Kessler, and L. M. Sander, Phys. Rev. Lett. **66**, 3032 (1991).

[2] J. W. Gibbs, *On the Equilibrium of Heterogeneous Substances*, The Collected Works of J. Williard Gibbs (Longmans, Green and Co., New York, 1928), p. 184.

[3] C. Herring, in *Structure and Properties of Solid Surfaces*, edited by R. Gomer and C. S. Smith (University of Chicago Press, Chicago, 1953), p. 5.

[4] H. Gao, J. Mech. Phys. Solids **42**, 741 (1994).

[5] A. E. H. Love, *A Treatise on the Mathematical Theory of Elasticity* (Dover, New York, 1927), Chap. 10.

[6] A. A. Bukharaev, A. A. Bukharaeva, N. I. Nurgazizov, and D. V. Ovchinnikov, Tech. Phys. Lett. **24**, 863 (1998).